PAPER • OPEN ACCESS

Train-based differential eddy current sensor system for rail fastener detection

View the article online for updates and enhancements.

Train-based differential eddy current sensor system for rail fastener detection

Praneeth Chandran[1,3] [iD]**, Matti Rantatalo**[1]**, Johan Odelius**[1]**, Håkan Lind**[2] **and Stephen M Famurewa**[1]

[1] Division of Operation and Maintenance, Lulea University of Technology, Luleå, Sweden
[2] Bombardier Transportation, Stockholm, Sweden

E-mail: praneeth.chandran@ltu.se

CrossMark

Abstract

One of the crucial components in rail tracks is the rail fastening system, which acts as a means of fixing rails to the sleepers to maintain the track gauge and stability. Manual inspection and 2D visual inspection of fastening systems have predominated over the past two decades. However, both methods have drawbacks when visibility is obscured and are found to be relatively expensive in terms of cost and track possession. The present article presents the concept of a train-based differential eddy current (EC) sensor system for fastener detection. The sensor uses the principle of electromagnetic induction, where an alternating-current-carrying coil is used to create an EC on the rail and other electrically conductive material in the vicinity and a pick-up coil is used to measure the returning field. This paper gives an insight into the theoretical background and application of the proposed differential EC sensor system for the condition monitoring system of rail fasteners and shows experimental results from both laboratory and field measurements. The field measurements were carried out along a heavy-haul railway line in the north of Sweden. Results obtained from both the field measurements and from the lab tests reveal that that the proposed method was able to detect an individual fastening system from a height of 65 mm above the rail. Furthermore, missing clamps within a fastening system are detected by analysing a time domain feature of the measurement signal.

Keywords: fastener, clamps, differential eddy current sensor, detection, inspection

(Some figures may appear in colour only in the online journal)

1. Introduction

In view of the mobilization and transportation of people and commodities, rail transportation plays a significant role. In addition, rail transportation forms a major contributing factor in the economic and industrial development of a nation. Railway infrastructure involves a huge investment and, with approximately £15–20 billion per annum spent on railway asset maintenance [1], maintenance managers are striving to cut maintenance costs through effective condition-based maintenance. Railway track issues are responsible for nearly half of all delays to passengers, mainly due to the downtime arising from railway track maintenance and renewal of networks [2]. Fasteners play a crucial role in the railway track system as they connect the rail to the sleepers, preventing the rail from moving and preserving the designed geometry of the track. Fasteners, with the help of rail pads, contribute to the dynamic behaviour of the track, transferring and damping the rail-wheel contact force to the lower parts of the infrastructure [3, 4]. Fasteners also maintain the gauge and prevent the rails from moving longitudinally and laterally relative to the sleepers. Failures of fasteners reduce the safety of train operations and may lead to catastrophic accidents [5]. Thus, to ensure the safety and high reliability of the track, fasteners

have to be inspected periodically. Traditionally, trained inspectors, who would walk along the track length and search for rail damage, carried out the task of fastener inspection. Manual inspection is slow, labour intensive and can sometimes introduce human errors in the inspection, as well as posing safety issues for the maintenance staff. Further, this method is expensive and time consuming for railroad companies specifically for long-term and large-scale development. Recent development in technology has seen automated visual inspection along with manual inspection being utilised for rail fastener inspection.

In Sweden, the inspection intervals for railway assets are based on track class, which is defined based on the individual traffic load and speed associated with it. There are seven such track classes, as shown in figure 1, and their conditions/descriptions are given in table 1. The number of inspections assigned in a year is higher for classes B4 and B5 as they are subjected to high load and speed throughout the year.

Table 2 shows the estimated time spent (in hours) and the cost incurred (in Euros) for inspection on two lines with a total track length *ca*. 300 km over a period of seven years. The inspection time and cost are estimated based on the inspection report from 2008 to 2014 for two lines on the northern and southern ends of the heavy-haul line in Sweden (section 111 and section 118, respectively). The sections cover a distance of 130 km and 164 km, respectively. The labour cost for the inspection was set, as an average value, at 60 Euros per hour, and an average inspection speed of 2 km h^{-1} was used. The inspection duration is estimated for all the inspection activities carried out on the tracks for both the sections. The cost of inspection is directly related to the inspection time, as clearly visible from table 2. Based on these estimates, the average annual cost for track inspection on both lines is over 110 000 Euros per line. By 2014 the cost of inspection was 42.7% above the average for a section in the northern loop and 72.5% above the average cost for that in the southern loop.

Table 3 shows a comparison of the time and cost involved in the inspection of track components with that of the overall track inspection, for both lines. The track components considered for this graph include all the components in a railway track that exhibit magnetic characteristics (rail, fastening system, weld joints, etc); overall track inspection takes into consideration those components that exhibit both magnetic and nonmagnetic properties. On average 76.5% of the overall time and capital for track inspection are used for inspecting track components such as rail surface, fastening systems, weld joints and switches and crossings. In 2014, 1961 h and over 235 000 Euros were spent on inspecting these track components along both sections, which accounts for 78.9% of the overall inspection cost (including both track and turnout inspection).

With the extension of high-speed railway networks, the major challenge lies in reducing these operation and maintenance costs while augmenting the capacity of the rail network. In order to lower maintenance costs, enhance safety and increase track capacity, railroad companies are laying more emphasis on substituting the current manual inspection process with automatic fastener inspection system for more
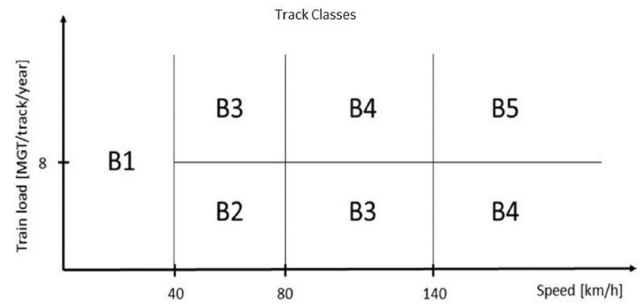

Figure 1. Track class with respect to train load in million gross tonnage and speed in km h^{-1}.

efficient, effective and objective inspections. Over the past two decades machine vision methods have been tested and applied to automate the inspection and detection for fastening systems [6–27].

Machine vision has been gradually adopted by the railway industry as a track inspection technology, since the pioneering work by Trosino *et al* [6, 7]. These first-generation visual inspection systems were capable of off-line analysis, i.e. collecting and storing images of rail for later review. However, these systems failed to facilitate automated detection in the early 2000s due to lack of fast processing hardware. In 2007, Marino *et al* introduced their VISyR system, which was a fully automatic and configurable FPGA-based vision system [8, 9] for real-time infrastructure inspection, able to analyze rail defects and to detect the presence/absence of the fastening bolts that fix the rails to the sleepers. The system was able to acquire images of the rail by means of a Dalsa Piranha 2 line scan camera (Matrox) with 1024 pixel resolution and using the Cameralink protocol. The system uses two 3-layer neural networks (NN) (running in parallel to detect hexagonal-headed bolts). To indicate the fastener, a binary output was generated, by taking a 2-level discrete wavelet transform (DWT) of a 24 × 100 pixel-sliding window (their images use non-square pixels) for the two networks as an input. The first NN uses Daubechies wavelets, while the second one uses Haar wavelets; these wavelet decompositions are equivalent to performing edge detection at different scales with two different filters. The same set of samples were used to train both networks and the final decisions were made based on the maximum output of each network. The VISyR system was successfully able to detect the presence/absence of fasteners.

In 2009 Babenko [10] used an image-based detection device comprising two industrial laser range scanners (one for each rail) to detect missing or defective fasteners. A convolutional filter bank was applied directly on these intensity images. Each type of fastener had a single filter associated with it, whose coefficients were calculated using an illumination-normalized version of the Optimal Trade-off Maximum Average Correlation Height (OT-MACH) filter [11]. Resendiz *et al* [12] adopted a track cart to capture video of railroad track with off-the-shelf cameras and recorded these data to an onboard laptop. To determine the location of rail components such as crossties and turnouts a texture classification with a bank of Gabor filters followed by an SVM was adopted. The MUSIC algorithm was encompassed to locate spectral

Table 1. Description of track classes in Sweden based on speed and load.

Track class	Speed (km h^{-1})	Load (MGT/track/year)
B1	Less than or equal to 40	—
B2	Higher than 40 but less than or equal to 80	⩽8
B3 (option 1)	Higher than 40 but less than or equal to 80	>8
B3 (option2)	Higher than 80 but less than or equal to 140	⩽8
B4 (option1)	Higher than 80 but less than or equal to 140	>8
B4 (option2)	>140	⩽8
B5	>140	>8

Table 2. Inspection time and cost of inspection for section 111 and section 118.

Year	Section 111		Section 118	
	Inspection time (hours)	Cost of inspection (Euros)	Inspection time (hours)	Cost of inspection (Euros)
2008	874	104 920	726	87 160
2009	987	118 480	762	91 490
2010	829	99 580	674	80 920
2011	805	96 620	1075	12 900
2012	909	109 160	910	109 240
2013	756	90 760	874.5	104 940
2014	1322	158 860	1643	197 180

Table 3. Inspection time and cost of inspection for overall track inspection and track components (with magnetic properties).

Year	Overall track inspection		Track components	
	Inspection time (hours)	Cost of inspection (Euros)	Inspection time (hours)	Cost of inspection (Euros)
2008	1228	147 360	994	119 280
2009	1295	155 400	1122	134 640
2010	1077.5	129 300	831.5	99 780
2011	1375.5	165 060	1029.5	123 540
2012	1288	154 560	893.5	107 220
2013	1195.5	143 460	828.5	99 420
2014	2484	298 080	1961	235 320

signatures to define expected component locations. Mao *et al* [13] used structured light sensors to inspect for damaged and loose fasteners and used a decision tree classifier to classify the defects in detail.

Visual inspection of fasteners has predominated over the past two decades, but the detection methods have varied over time. Marino *et al* [8] used a multilayer perceptron neural classifier to detect missing hexagonal-headed bolts. Stella *et al* [14] used a neural classifier to locate missing fasteners (hook-shaped), employing wavelet transform and principal component analysis. Yaang *et al* [15] adopted a direction field as the template of a fastener and matched it using linear discriminant analysis to obtain the weight coefficient matrix. Ruvo *et al* [9], adopted an error backpropagation algorithm to model mainly two type of fasteners. To achieve real-time performance a detection algorithm was implemented on a graphical processing unit. For automatic detection of hexagonal bolts, Ruvo *et al* [16] also adopted a FPGA-based architecture using the same algorithm. Xia *et al* [17] used AdaBoost training for hook-shaped fasteners, dividing the fastener into four parts and training each with AdaBoost, thus enabling it to detect worn out fasteners. Fan *et al* [18] adopted a line local binary pattern encoding method that considers the relationship between the

center point and its upper and lower neighborhoods, enabling them to represent the key components of fasteners. Li *et al* [19] and Rubinsztejn [20] used the same algorithm to detect fasteners and their components. Gabor filters [21], edge-detection methods [22], and support vector machines (SVMs) [23] are some of the other widely used techniques for modelling and detecting fasteners. Common generative models used for fastener detection include latent Dirichlet allocation (LDA) [24] and structure topic models (STMs), which are an extension of LDA. Feng *et al* [25] used a STM to model fasteners, as it was able to learn the probabilistic representations of different objects using unlabelled samples. Recent advancements have seen the application of deep learning for automated fastener detection from image processing [5, 26, 27].

Automated visual inspection is a relatively expensive technique to carry out, especially for long-term projects and long-distance measurements. The optimum condition for detection of different fasteners and their complicated geometry make this technique less effective. Automated visual inspection becomes a challenge when the fastener and the rail are obscured due to dust coverage, surface erosion and rusting. Another drawback of this method is its lack of ability to detect the rail surface and the fasteners covered by snow, stones and

other debris or during heavy rain. This calls for additional rail surface treatment or removal processes that add to the expense of the railroad companies. Further, visual-based sensors are difficult to mount and maintain on in-service trains as they are integrated in the operation and affected by brightness fluctuation and motion blurring during travel. Therefore, an effective and sophisticated alternative approach for fastener inspection needs to be explored.

Non-destructive testing (NDT) plays an important role in condition-based maintenance (CBM) of railways. Eddy current (EC) testing is one of several NDT methods that use the principle of electromagnetism for examining a component. Eddy-current-based inspection can overcome the major challenges mentioned above. The presence of non-conductive materials in the sensor-to-target gap do not affect the EC sensors. This allows their use in dirty environments, such as those involving water, oil, snow and machine fluids, where other displacement sensor technologies fail. Another advantage of this technique is that there is minimal, or no, need for surface treatment. This paper presents the concept of a sensor for fastener detection using the principle of EC testing.

The proposed differential EC sensor concept and principle are discussed in section 2 with special attention to its application in rail vehicles. The experimental method carried out for lab and field tests are explained in section 3. Finally, the results from both lab and field tests are presented in section 4.

2. Differential eddy current sensor—Lindometer

The eddy current method has been well known for decades in the non-destructive testing of electrically conductive objects [28]. EC testing is based on the physical phenomenon of electromagnetic induction, where an oscillating magnetic field is generated by passing an alternating current through a coil. Every coil is characterized by an impedance Z_i, which is a complex valued generalization of resistance, for a single frequency sinusoidal excitation f:

$$Z_i = \frac{V_i}{I_i} = R_i + jX_i \tag{1}$$

where V_i and I_i are the voltage and current across the coil, R_i is the resistance and X_i is inductive reactance of the coil with an inductance of L_i. The impedance Z_i has a magnitude $|Z|$ and phase φ:

$$Z_i = R_i + jX_i \, (\text{where } X_i = 2\pi f L_i) \tag{2}$$

$$|Z| = \sqrt{R_i^2 + X_i^2} \tag{3}$$

$$\varphi = \tan^{-1}\left(\frac{X_i}{R_i}\right). \tag{4}$$

A time-varying magnetic field is generated when an alternating current is fed to a conducting coil. EC inspections are based on Faraday's law of electromagnetic induction that states that an alternating magnetic induction flux density induces a circular current in an electric conductor. The electromotive force

ε is proportional to the change of magnetic induction flux density over time:

$$\varepsilon = -\frac{d\phi_B}{dt}. \tag{5}$$

The induced circular current, known as the EC, creates a secondary magnetic field, which tends to cancel out the driving field at the local point of the surface. The secondary magnetic field has a weakening effect on the primary magnetic field and hence the new imaginary part of the coil impedance decreases as the EC intensity increases in the test piece. The real part of the coil impedance also changes as the EC contributes to the increase of the power dissipation of energy:

$$Z_f = \frac{V_f}{I_f} = R_f + jX_f. \tag{6}$$

EC inspection typically measures this coil impedance change from Z_i to Z_f in the form of either voltage or current signals to reveal specific information of the test piece. EC flow is more concentrated near the surface and is not uniformly distributed throughout the entire volume of the test piece. The current flow decreases exponentially as the distance from the surface increases. The skin depth δ is the distance from the surface at which the EC density decreases to a level of '$1/e$' of its surface value and is given by

$$\delta = \sqrt{\frac{2}{\mu\omega\sigma}} \tag{7}$$

where σ is the conductivity given by the reciprocal of resistivity $\sigma = 1/\rho$, $\omega = 2\pi f$ and μ is the magnetic permeability $\mu = \mu_r\mu_o$. In principle, EC sensors are sensitive to local fluctuations of the conductivity (σ), magnetic permeability (μ) and geometric form of the material. Hence, such sensors can be used to detect inhomogeneities along the rail track, e.g. rail fasteners and irregularities of the rail [28].

For applications in train-based measurements, differential EC sensors are preferred. The differential EC sensor used in this study was developed at Bombardier Transport (Sweden) and was named the 'Lindometer'. Figure 2 shows the proposed sensor consisting of driver coil 'D' and two pick-up coils 'P1' and 'P2'. The driving coil is driven by a sinusoidal primary current $i(t)$, which generates an alternating primary magnetic field. ECs are thus induced within the rail and other electrically conductive material located in the proximity of the sensor. A secondary magnetic field is generated as a result of these ECs, which has an opposite direction to the primary field, complying with Lenz's law. The Lindometer encloses two such independent EC sensors, placed at a distance of 20 cm apart.

The Lindometer uses two driving fields at frequencies of 18 kHz and 27 kHz, respectively, to detect variations in amplitude, phase and a combination of both. Two channels were installed to facilitate future speed measurements using cross-correlation techniques. However, in this study the two channels were used to increase the detection probability of the system. The abovementioned frequencies are taken as the carrier frequencies, as these frequencies fall under the rail norms.
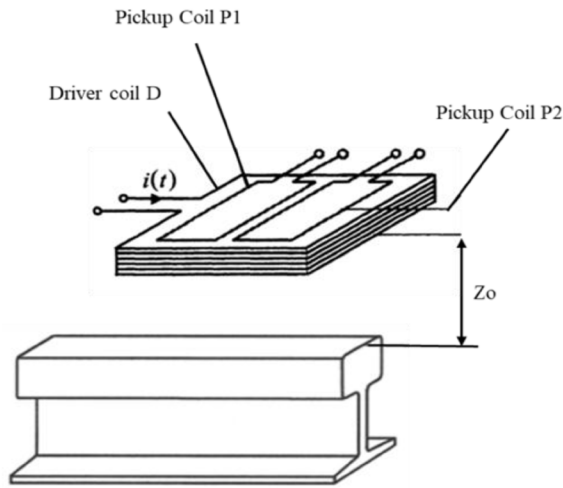
Figure 2. Arrangement of a differential eddy current (EC) sensor coil measuring over a rail head.

The information along the rail is represented as variations in amplitude or phase or a combination of both, which are extracted and analyzed by demodulation techniques. For each sensor the signal is multiplied by its carrier frequency and low-pass filtered (2 kHz) to demodulate the signal and extract the base band. The signal is also resampled from 215.52 kHz to 35.92 kHz. The size of each driving coil is approximately 18 (z), 70 (x), and 155 (y) mm. The driving coil acts as an outer winding, enclosing the pick-up coils. The winding is applied in one layer with $N = 22$ turns with a copper wire of 0.7 mm diameter. The pick-up coils have a dimension of 18 (z), 30 (x) and 150(y) mm, and each coil has a winding applied in one layer with 94 turns and a copper wire of 0.16 mm diameter. The two coils are placed side by side in the x-direction with a gap of 4 mm in the centre of the coil system, for both sensors.

To get an approximation of the primary magnetic field strength B_z just above the rail head, we transfer the rectangle area of the sensor (155 × 70) to a circular coil with a diameter of 118 mm. The magnetic flux density on the axis of a circular current filament of radius a with current I can be determined using the magnetic scalar potential on the same axis. The magnetic scalar potential V_M at a point M (see figure 3) on the loop axis is given by

$$v_M = \frac{I}{4\pi}\Omega \tag{8}$$

where Ω is the solid angle at M, made by the contour. The solid angle is equal to the area cut out of a sphere of unit radius, centered at the apex, that the object covers and is given by

$$\Omega = \frac{S}{r^2} \tag{9}$$

where S represents the area cut of the sphere with radius r, and is given by

$$S = 2\pi r^2(1 - \cos\theta). \tag{10}$$

Substituting the area in equation (9) for the solid angle, we get
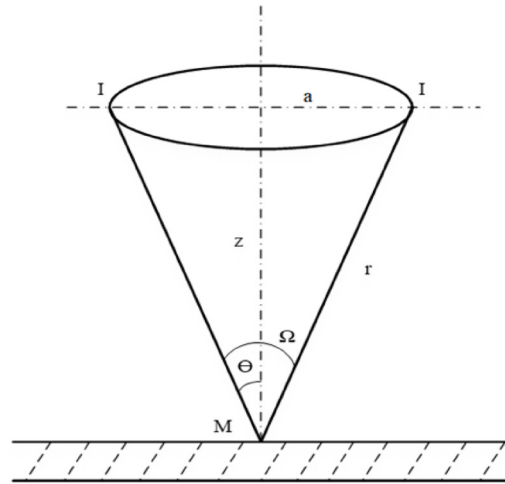

Figure 3. Magnetic scalar potential at a point M on the loop axis due to a circular current-carrying coil.

$$\Omega = \frac{2\pi r^2\,(1 - \cos\theta)}{r^2} \tag{11}$$

$$\Omega = 2\pi\left(1 - \frac{z}{\sqrt{a^2 + z^2}}\right). \tag{12}$$

Substituting the solid angle in equation (8):

$$V_M = \frac{I}{2}\left(1 - \frac{Z}{\sqrt{a^2 + z^2}}\right). \tag{13}$$

Further, the magnetic flux density can be estimated by calculating the gradient of the magnetic scalar potential:

$$B = -\mu_0 grad V_M. \tag{14}$$

However, due to symmetry the magnetic flux density vector has only z-component in our case:

$$B_z = -\mu_0\frac{\partial V_M}{\partial z} \tag{15}$$

$$B_z = \frac{\mu_0 I}{2}\frac{a^2}{(a^2 + z^2)^{3/2}} \;(\text{ for } N = 1 \text{ turn}) \tag{16}$$

$$B_z = \frac{\mu_0 IN}{2}\frac{a^2}{(a^2 + z^2)^{3/2}} \;(\text{for } N \text{ turns}). \tag{17}$$

From the above equation we get a magnetic field strength of 213 μT on the rail surface at a distance of 65 mm (z) from the sensor when a current of 3A (I) flows through the coil with 22 turns (N). We assume the EC as a small current-carrying contour much less in geometry ($a \ll z$) than the distance to the pick-up coils. Thus the secondary magnetic field (B_{sec}) caused by the local EC decreases with a power of three of the distance to the pick-up coils:

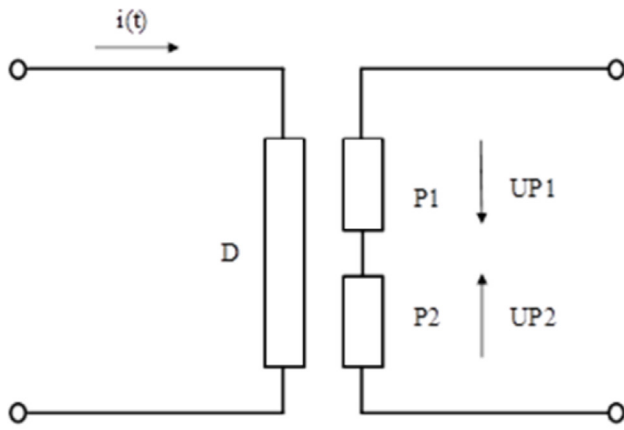$$B_{sec} \approx \frac{\mu_0 I}{2}\frac{a^2}{z^3} \;(\text{if } a \ll z). \tag{18}$$

Figure 4. Circuit diagram of the sensor system.

Figure 5. Magnetic flux along the *x*-axis due to the driving coil.

$$B = \frac{\mu_0 I}{2} \frac{a^2}{(a^2 + z^2)^{3/2}} \cos \theta. \tag{21}$$

The two pick-up coils are enclosed by the driving coil and differentially coupled for each of the sensors, as depicted in figure 4. The two frequencies have a common factor of 9 kHz, which gives the opportunity to cancel out the small cross-talk between them by the inbuilt cross-talk cancellation (CTC) function within the sensor. The differentially coupled pick-up coils cancel out the direct cross-talk between the driver and pick-up coil, though not completely. The resulting voltage $u(t)$ is the result of the cross-talk residue and the induction of ECs along the rail, which are linearly superimposed. The quality of the cross-talk cancellation is a question of the geometrical symmetry between the three coils, and hence the windings are placed in an even layer with no crossovers. The entire unit is vacuum potted with epoxy resin to stabilize the sensor, both against vibrations and to reduce temperature drift.

The driving coil generates an EC in the rail and vicinity in the x–y plane. The pick-up coils are sensitive only to the z-component of the generated flux from the EC due to the geometrical orientation, as shown in figure 2. The differentially coupled pick-up coils (P1–P2) are sensitive only to changes in the EC in the rail and its vicinity. If there is an even surface with no change in the conductivity (σ), magnetic permeability (μ) or geometric form of the material, as an ideal rail with no clamps or any surface defects, the resulting voltage $u(t)$ will be zero due to induction of similar ECs all over the place. An EC change happens when there is a change in μ or σ or geometry at one single point at the railhead, while other parts remains the very same. Due to the symmetry of the differentially coupled pick-up coils, only the singular point with the EC change will create a signal (for both the sensors) given by the equations below:

$$u(t)_{18} = P1v(t)_{18} - P2v(t)_{18} \tag{19}$$

$$u(t)_{27} = P1v(t)_{27} - P2v(t)_{27}. \tag{20}$$

The resulting signal $u(t)$ will be a function of the relative distance between the single-point EC source and two pick-up coils. In the x-direction, we must also consider the angle Θ (refer to figure 5) where the driving flux density varies significantly along the x-axis. Hence, at a distance of $\pm a$ from the origin the magnetic field is given as
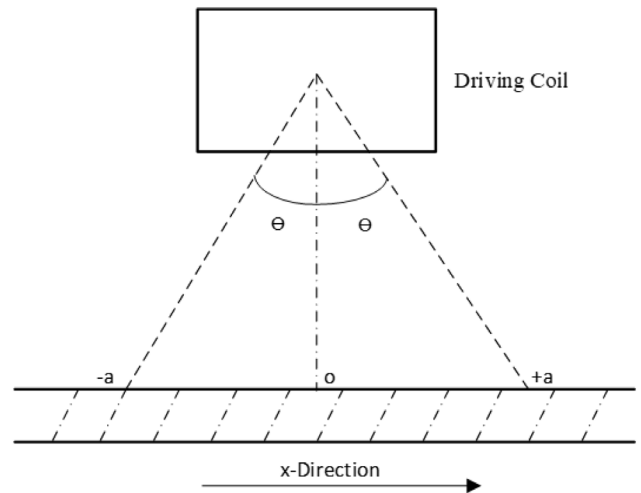
Due to the symmetry of the differentially coupled pick-up coils, there is zero induction $u(t)$ when the source is just below the symmetry line of the pick-up coil (figure 6(a)), positive induction to the left (figure 6(b)), and negative induction to the right (figure 6(c))

3. Experimental method

For both the field and laboratory test, the sensor was mounted 65 mm above the rail head (refer to figures 7 and 8(a)) on a trolley system and was pushed along the track (speed was not set to be uniform). The sensor was powered using a 12V62AH battery and the measurements were recorded using a laptop.

3.1. Laboratory tests

Laboratory tests were carried out to test the measurement system under well-defined conditions and in a controlled environment. In particular, the response of the sensor to detect a clamp at various distances from the rail was tested in the laboratory. The clamp was placed at a lateral distance ranging from 0 to 180 mm from the rail, as shown in figure 7, and measurements were recorded for the same.

3.2. Field tests

Field measurements were performed along the northern loop of the heavy-haul line at Katterjåkk and Stordalen, close to the Sweden-Norway border, which was considered for the above discussion (refer to section 1). The most frequently observed fault in the fastening system along this section was the absence of clamps from system. Different measurements were conducted along the railway track, with healthy track sections having intact e-clip fasteners, and were compared with measurements of a section with missing clamps.
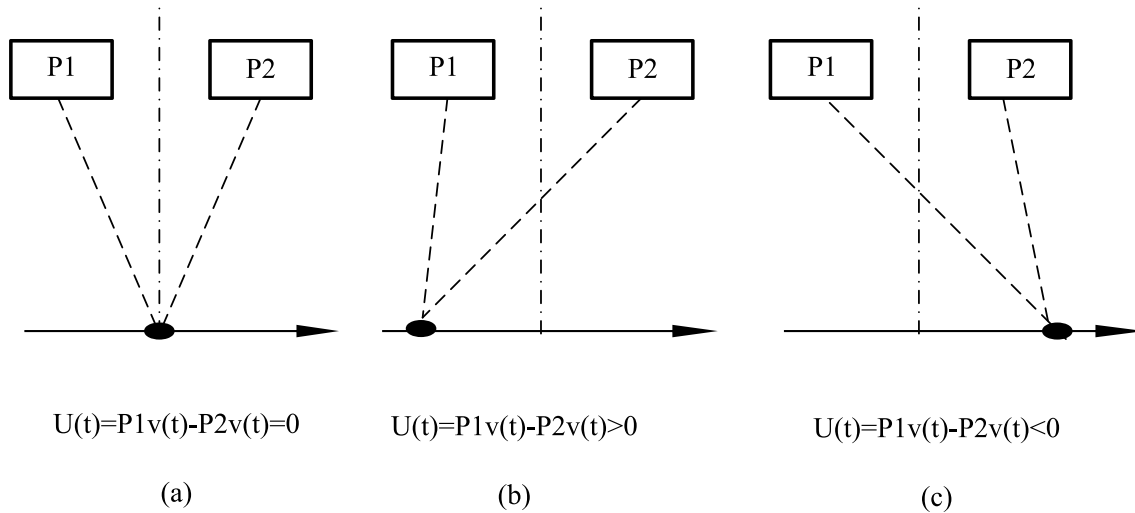
$$U(t) = P1v(t) - P2v(t) = 0 \qquad U(t) = P1v(t) - P2v(t) > 0 \qquad U(t) = P1v(t) - P2v(t) < 0$$

(a)   (b)   (c)

Figure 6. Induction in the differentially coupled pick-up coils due to the position of current source. (a) Source at the symmetry line, (b) source to the left of the symmetry line, (c) source to the right of the symmetry line.
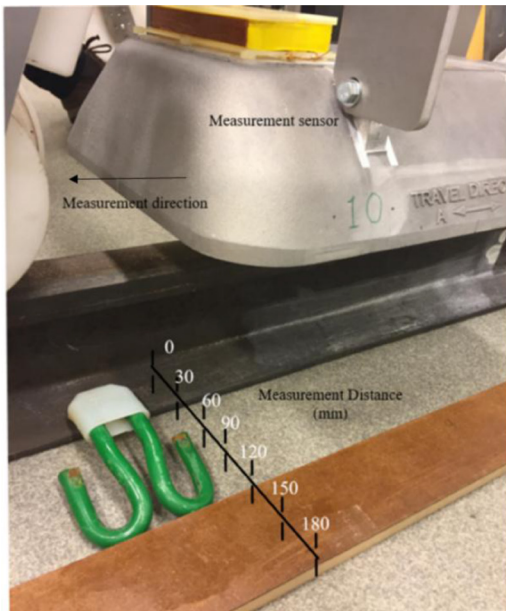

Figure 7. Measurement set-up (lab) for detecting clamps using the Lindometer sensor.

Figure 8(a) depicts the measurement trolley used to measure the fastening system along the track and figure 8(b) shows an e-clip fastening system with an intact clamp and with one missing clamp.

A controlled test pattern was carried out in the field to detect missing clamps from the e-clip fastening system, as depicted in figure 9. The clamps were removed from the outer part of the rail at the 20th sleeper, from the inner part at the 25th sleeper and from both inner and outer part at the 30th sleeper, from the start of the measurement.

3.3. Pre-processing

A number of pre-processing methods were required before sufficient information could be established about the fastener system from the raw signal. The EC signal had to be filtered

in order to extract information pertaining to only the fastening system. Further, the signals had to be demodulated so that the fastener signature was in the phase direction, maximizing the signal output in the real axis.

3.3.1. Filtering. The periodicity of the fasteners in the signal was found to be lower than 3 Hz. Hence the EC signal was filtered using a low-pass filter of 3 Hz, so as to retrieve information regarding fastening system along the rail and attenuate other frequency components that correspond to noise or other components of the rail.

3.3.2. Rotation of EC signal. The fastener signatures were found to be shifted from the in-phase direction, and in order to extract maximum information and have better visualisation, the fastener signature had to be rotated such that these signatures were projected along the in-phase direction (real part). This also helps in suppressing other responses not pertaining to fasteners, to an extent. The method used to rotate the EC pattern was based on the observation that the peak amplitude of an individual fastener signature was maximum when the fastener signatures were aligned along the in-phase direction. The complex EC signal was rotated by a degree Θ or Φ radian, such that the peak amplitude of the fastener signatures were maximised.

4. Results and discussions

4.1. Lab test results

Figure 10 shows the time signal of the measurement carried out in the lab to capture clamp signatures over various distances from the rail for the 18 kHz channel. The clamp signature is measured in terms of induced voltage (*y*-axis) with respect to time (*x*-axis). The sensor was able to detect the clamp from a vertical distance of 65 mm from the rail surface. The signal achieved the highest amplitude when the clamp distance from the rail was zero (mm). The clamp signature

Figure 8. (a) Lindometer measurement system setup, (b) e-clip fastening system, intact and with a missing clamp.
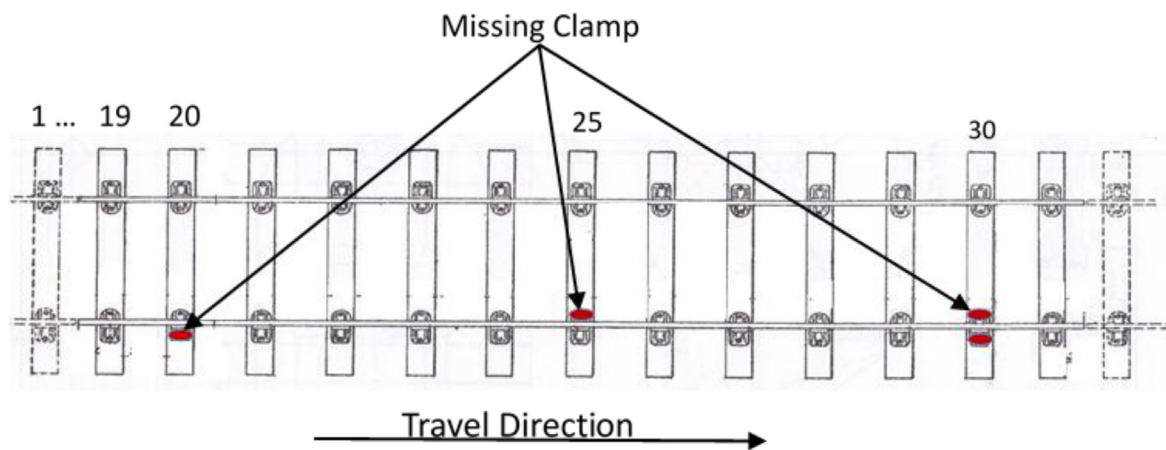

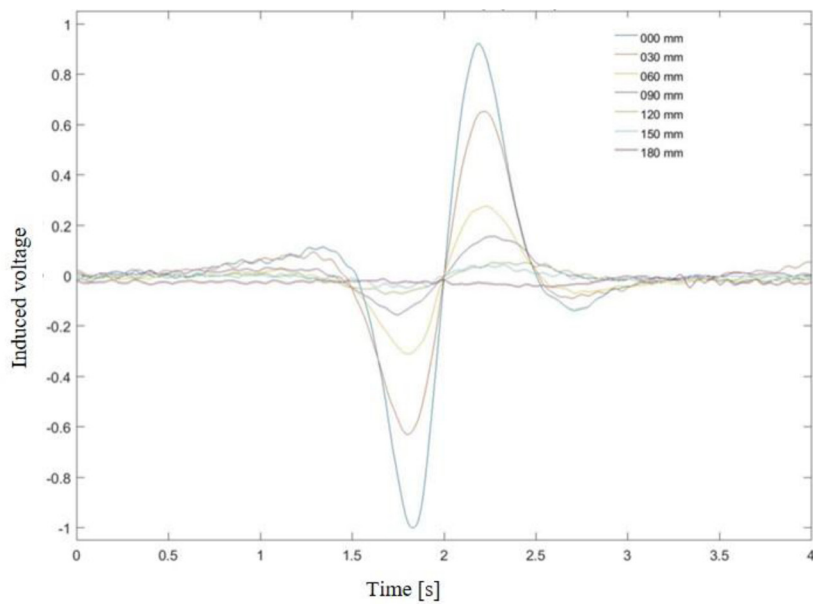**Figure 9.** Measurement pattern to detect missing clamp.

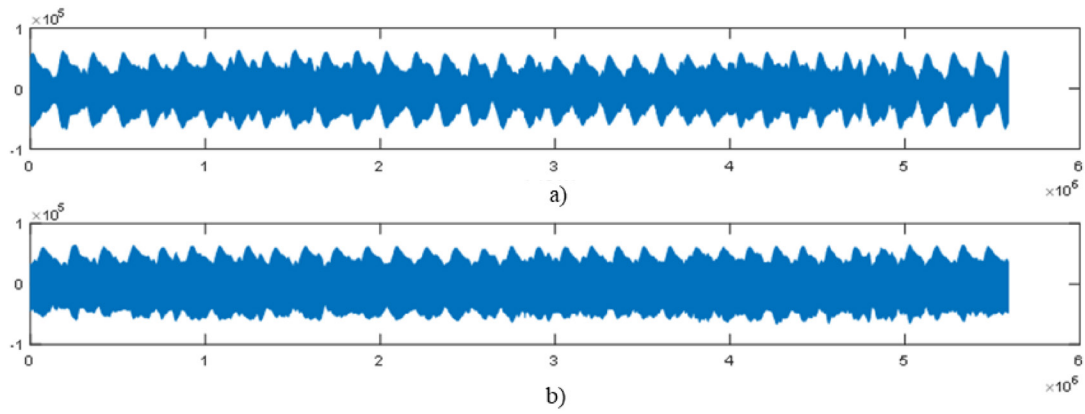**Figure 10.** Clamp signature with respect to the distance from the rail.
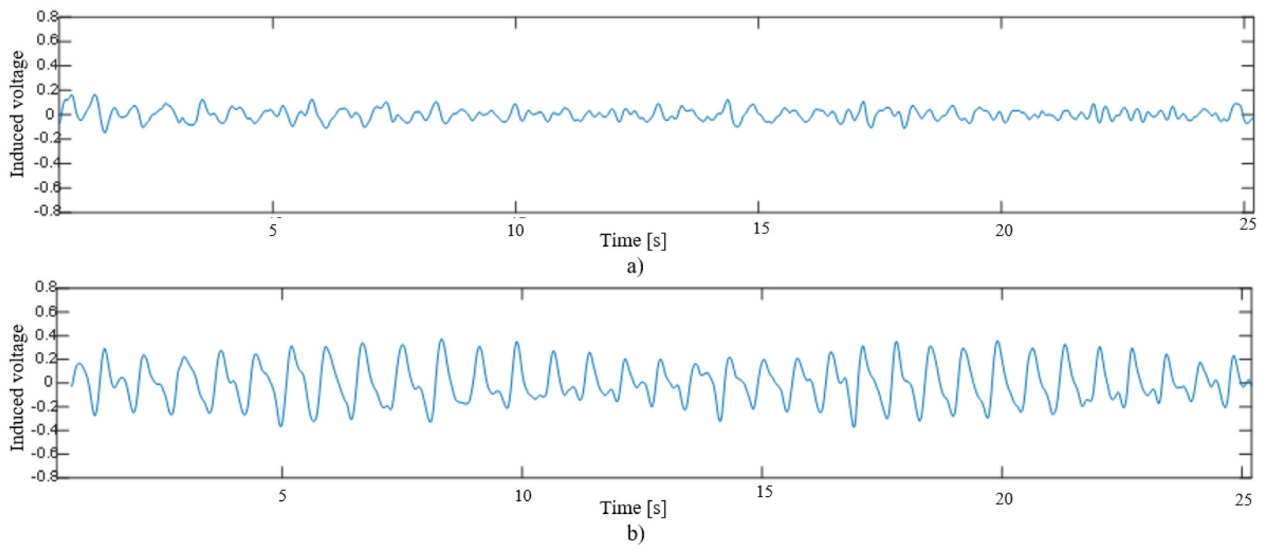
Figure 11. Raw signal: (a) 18 kHz, (b) 27 kHz.

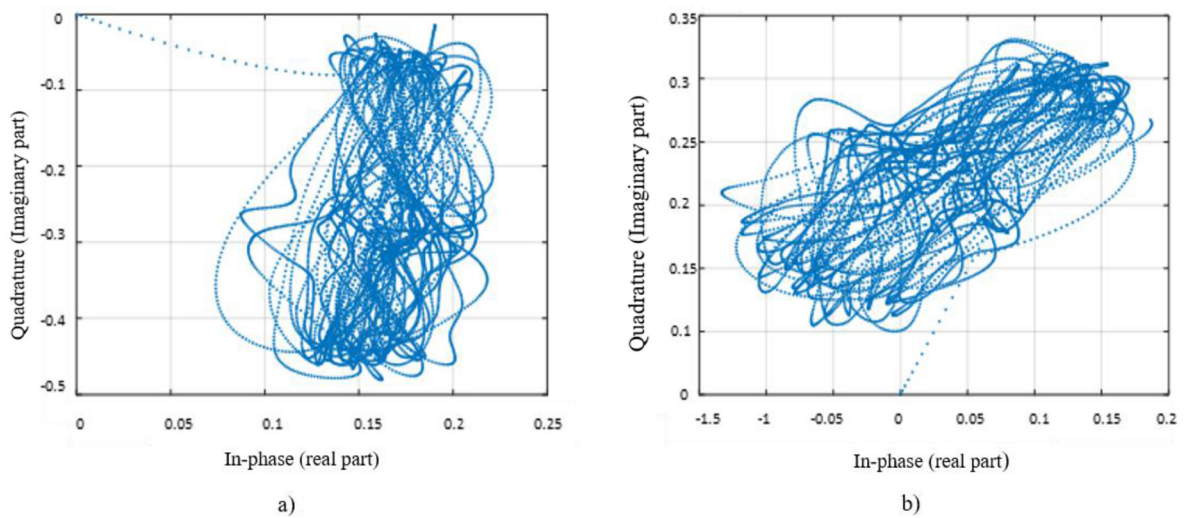**Figure 12.** Time signal: (a) 18 kHz, (b) 27 kHz.

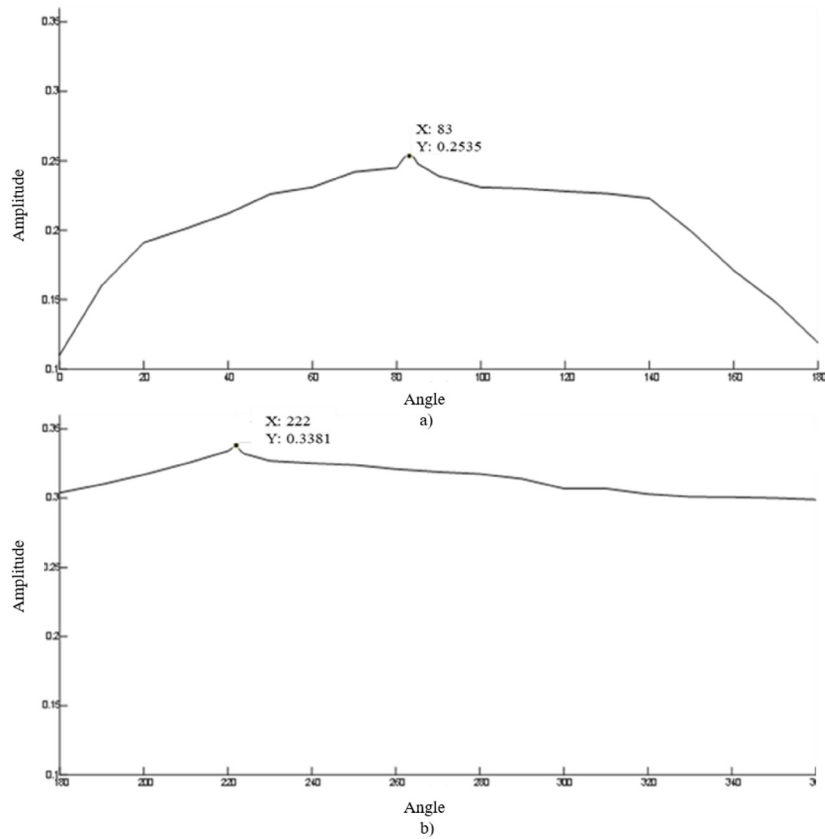**Figure 13.** IQ plot of the time signal: (a) 18 kHz, (b) 27 kHz.

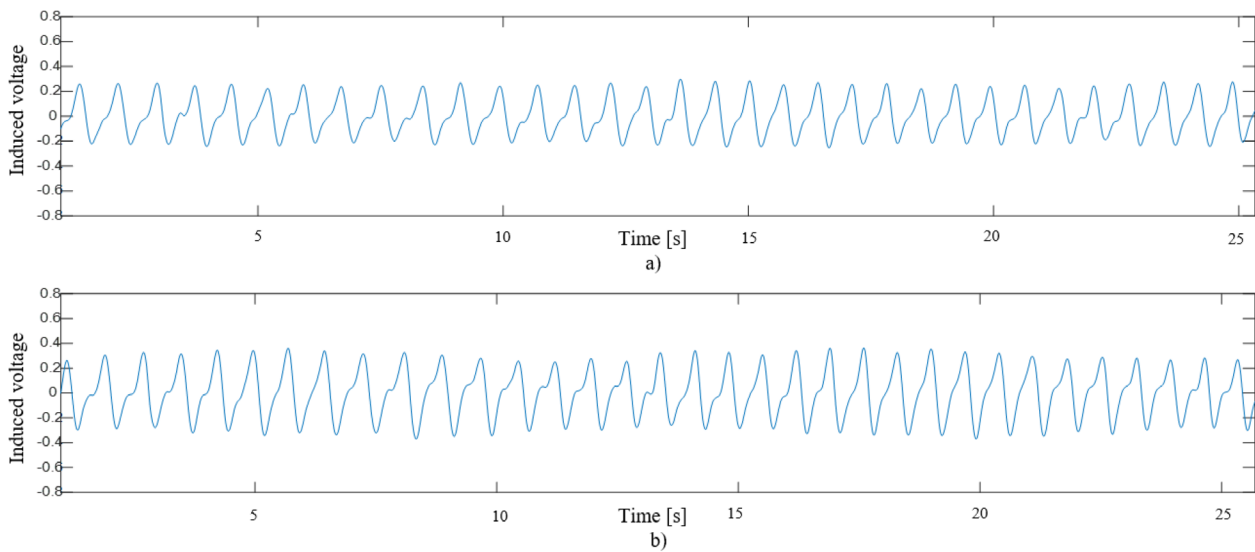**Figure 14.** Optimum demodulation angle: (a) 18 kHz, (b) 27 kHz.

Figure 15. Time signal after applying demodulation angle: (a) 18 kHz, (b) 27 kHz.

reduced as the horizontal distance between the rail and the clamp increased. The measurements also show that the signal strength is approximately zero as the clamp is out of the scope of view of the sensor. From the results, it can be inferred that the sensor is effective in detecting the fastening systems and can be used to detect loose and missing components from a fastening system.

4.2. Field test results

Figure 11 depicts the raw signal obtained from the sensor, for both the 18 kHz and 27 kHz driving fields. The above measurements were recorded over 33 sleepers, without significant surface defects.

Figure 12 represents the time signal of the raw signal for both the driving field after demodulating the raw signal with an
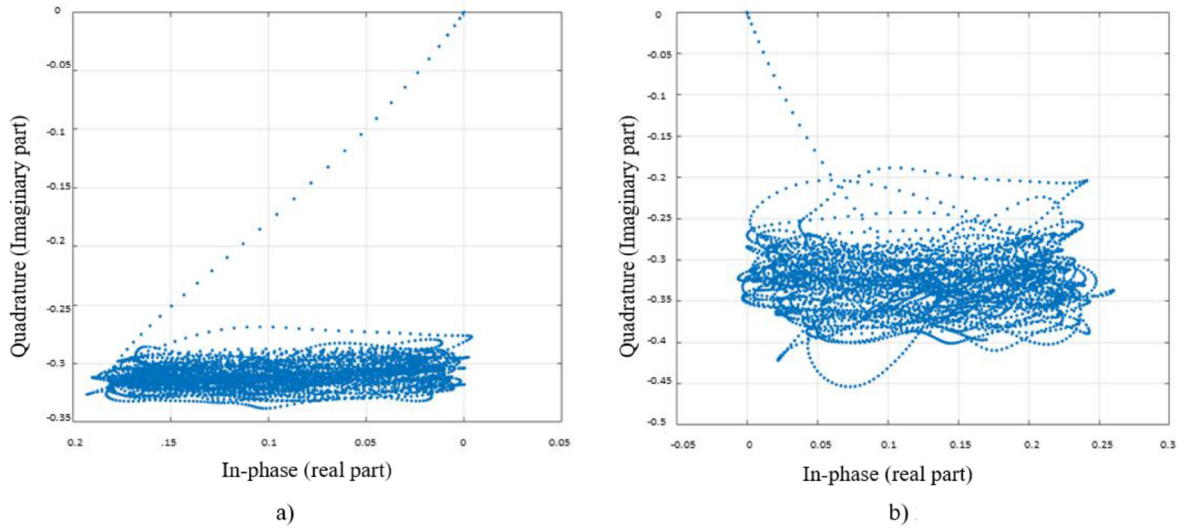
Figure 16. IQ plot after demodulating the signal: (a) 18 kHz, (b) 27 kHz.
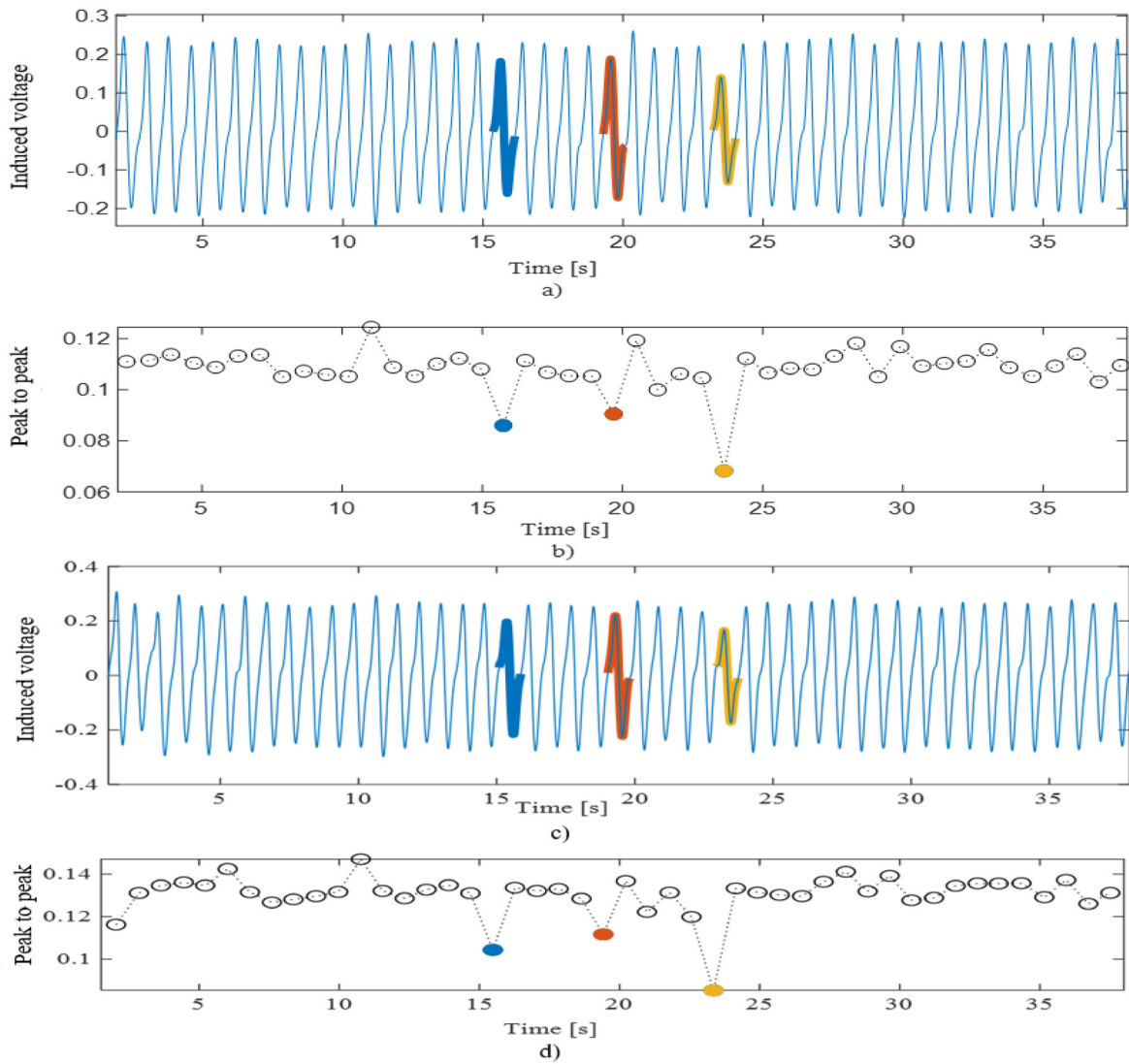

Figure 17. Measurement to detect missing clamps: (a) time signal for 18 kHz, (b) peak to peak plot for 18 kHz, (c) time signal for 27 kHz, (d) peak to peak plot for 27 kHz.

angle of 0° and using appropriate filters. The time signal plot shows a significant change in the output voltage, indicating fluctuations in either the magnetic permeability, conductivity or the geometric form, or a combination of all in the railhead and its vicinity. It becomes a relatively hard task to detect individual fastener signatures from the above time signal. The IQ plot of the signal (refer to figure 13) shows that the signals are modulated at a certain angle with respect to the in-phase or the real axis, hence choosing an optimum demodulation angle becomes essential in order to have a better visualization of the fastening system.

Figure 14 shows the plot of peak amplitude of an individual fastening system over various demodulation angles. The optimum demodulation angles were selected for both the driving field based on the maximum amplitude (of the peak) achieved for the fastening system. The highest amplitude for an individual fastener was achieved at an angle of 83° and 222°, respectively, for the two carrier frequencies. At an angle corresponding to $\pm\pi$ with respect to these optimum demodulation angles, the fastener signature achieves a similar maximum amplitude but the signal becomes inverted. The signal was further analyzed based on this optimum angle.

Figure 15 depicts the time signal for both the driving fields after applying the optimum demodulation angle to the signal. Individual fasteners are easily distinguishable from both 18 kHz and 27 kHz plots. The zero crossing in the signal from the positive to negative values indicates the centre positioning of the fastening system for each sleeper. The plot also shows that a good correlation can be established between the two driving field signals with a time delay. The slight time delay is due to the distance between the two sensors within the measurement system. The IQ plot (refer to figure 16) shows that the fastener signatures are aligned in parallel with respect to the *x*-axis. A small band of features appears to deviate from the normal pattern in the IQ plot, which corresponds to the initial saturation of the sensor.

Figures 17(a) and (c) show the time signal for the 18 kHz and 27 kHz driving fields for the measurement carried out to detect missing fasteners (refer to figure 9).The fastener signature shows a drop in amplitude at those positions where the clamps were missing from the fastener. Both the positive and negative induction drops in the signal when the clamps are found to be missing. When both clamps are missing from the fastener, the amplitude of the fastener signature drops by approximately 41% from that of a fastener with intact clamps. A time domain feature was extracted for each fastener signature from the recorded measurement. A reduction in metallic material will reduce the induced current and hence the amplitude of the return field. For this reason, the peak-to-peak (P2P) was selected. Figures 17(b) and (d) show the P2P plot of individual fasteners in the measurement. A reduction of P2P values shows a correlation with the absence of one or two clamps from a fastener system. The P2P value significantly drops when there are two missing clamps within a fastening system. It can be inferred from these results that the sensor can be used to detect missing components from a fastening system from a height of 65 mm above the rail surface.

5. Conclusion and future work

Automated visual inspections are currently employed for rail and fastener inspection, despite the fact that these modes of inspection require huge investment. Further, these modes of inspection may not be reliable in adverse environmental conditions with snow/debris obscurity. An alternate approach using a train-based differential EC-based sensor is recommended in this paper. Measurements were carried out along a heavy-haul line in Sweden using the measurement system for this study, and the following conclusions can be drawn from the above results.

- The proposed inspection method, with a train-based measurement system using a differential EC sensor, can detect fastener signatures from a distance of 65 mm above the railhead. Individual fastener signatures are easily distinguishable from the 1D time signal plots for both the driving fields. This approach can provide faster scanning speeds with less track possession requirement and faster feedback.
- The time signal plots clearly show that a very good correlation can be achieved in the 1D signal between 18 KHz and 27 KHz signals, with a time delay. This correlation can be useful for speed measurements and position monitoring of the train.
- The demodulation angle remains the same for all the signal processing techniques for a particular fastening system as the geometrical shape, the magnetic permeability and the conductivity of the component remains the same. The demodulation angle can be used as a parameter to distinguish between different types of fasteners as different fastening systems have different geometrical shapes. This study will be carried out in future work.
- The study also shows that the missing clamps can be detected by analyzing the fastener signatures. Missing clamps cause a reduction in the metallic material and change the geometry of the fastening system, thus reducing the amplitude of the return field. A clear difference is noticed in the P2P value for a healthy fastener with intact clamps and when one or both clamps are missing.
- The work in this study was based on analyzing time domain features of the measurement signals. These features are subject to change when the distance between the sensor and the object varies (i.e. lift off effect). In this application, lift off can occur due to wheel wear. However, this is a slow-occurring process which can be handled by continuous automatic calibration of the system where healthy signatures are used as a reference. This study will be carried out in future work.

The future scope in this study also involves quantification of rail defects, detecting other magnetic track components and developing efficient condition monitoring techniques with the aid of machine learning techniques to detect and predict faults from big data.

Acknowledgments

ORCID iDs

Praneeth Chandran ⓘ https://orcid.org/0000-0002-2300-9716

References

[1] Lidén T and Joborn M 2016 Dimensioning windows for railway infrastructure maintenance: cost efficiency versus traffic impact *J. Rail Transp. Plan. Manage.* **6** 32–47

[2] Patra A P 2009 Maintenance decision support models for railway infrastructure using RAMS & LCC analyses *Doctoral Thesis* Luleå Tekniska Universitet

[3] Wang A, Wang Z, Zhao Z, Zhang Y, Duan Y, Lei T and Du M 2015 Effects of track stiffness and tuned rail damper on rail roughness growth and rail vibration levels on metro system *Noise and Vibration Mitigation for Rail Transportation Systems* (Berlin: Springer) pp 667–74

[4] Köstli K, Jones C and Thompson D 2008 Experimental and theoretical analysis of railway bridge noise reduction using resilient rail fasteners in Burgdorf, Switzerland *Noise and Vibration Mitigation for Rail Transportation Systems* (Berlin: Springer) pp 208–14

[5] Wang S, Dai P, Du X, Gu Z and Ma Y 2018 Rail fastener automatic recognition method in complex background *10th Int. Conf. on Digital Image Processing (Shanghai, China, 9 August 2018)* p 1080625

[6] Trosino M, Cunningham J J and Shaw A E III 2000 Automated track inspection vehicle and method *US Patent* 6 064 428

[7] Trosino M, Cunningham J J and Shaw A E III 2002 Automated track inspection vehicle and method, National Railroad Passenger Corp, 2002 *US Patent* 6 356 299

[8] Marino F, Distante A, Mazzeo P L and Stella E 2007 A real-time visual inspection system for railway maintenance: automatic hexagonal-headed bolts detection *IEEE Trans. Syst. Man Cybern.* C **37** 418–28

[9] De Ruvo P, Distante A, Stella E and Marino F 2009 A GPU-based vision system for real time detection of fastening elements in railway inspection *2009 16th IEEE Int. Conf. on Image Processing* (Cairo, Egypt, 7-10 November 2009) pp 2333–6

[10] Babenko P 2009 Visual inspection of railroad tracks *UMI Doctoral Dissertation Dessertation* University of Central Florida

[11] Mahalanobis A, Kumar B V, Song S, Sims S and Epperson J 1994 Unconstrained correlation filters *Appl.Opt.* **33** 3751–9

[12] Resendiz E, Hart J M and Ahuja N 2013 Automated visual inspection of railroad tracks *IEEE Trans. Intell. Transp. Syst.* **14** 751–60

[13] Mao Q, Cui H, Hu Q and Ren X 2018 A rigorous fastener inspection approach for high-speed railway from structured light sensors *ISPRS J. Photogramm. Remote Sens.* **143** 249–67

[14] Stella E, Mazzeo P, Nitti M, Cicirelli G, Distante A and D'Orazio T 2002 Visual recognition of missing fastening elements for railroad maintenance *The IEEE 5th Int. Conf. on Intelligent Transportation Systems, 2002. Proc.* pp 94–9

[15] Yang J, Tao W, Liu M, Zhang Y, Zhang H and Zhao H 2011 An efficient direction field-based method for the detection of fasteners on high-speed railways *Sensors* **11** 7364–81

[16] De Ruvo G, De Ruvo P, Marino F, Mastronardi G, Mazzeo P L and Stella E 2005 A FPGA-based architecture for automatic hexagonal bolts detection in railway maintenance *7th Int. Workshop on Computer Architecture for Machine Perception, 2005. CAMP 2005. Proc.* (Piscataway, NJ: IEEE) pp 219–24

[17] Xia Y, Xie F and Jiang Z 2016 Broken railway fastener detection based on adaboost algorithm *2010 Int. Conf. on Optoelectronics and Image Processing* pp 313–6

[18] Fan H, Cosman P C, Hou Y and Li B 2018 High-speed railway fastener detection based on a line local binary pattern *IEEE Signal Process. Lett.* **25** 788–92

[19] Li Y, Otto C, Haas N, Fujiki Y and Pankanti S 2011 Component-based track inspection using machine-vision technology *Proc. of the 1st ACM Int. Conf. on Multimedia Retrieval* (New York: ACM) p 60

[20] Rubinsztejn Y 2011 Automatic detection of objects of interest from rail track images *Masters of Science Dissertation* Faculty of Engineering and Physical Science, University of Manchester

[21] Mandriota C, Nitti M, Ancona N, Stella E and Distante A 2004 Filter-based feature selection for rail defect detection *Mach. Vis. Appl.* **15** 179–85

[22] Singh M, Singh S, Jaiswal J and Hempshall J 2006 Autonomous rail track inspection using vision based system *Proc. of the 2006 IEEE Int. Conf. on Computational Intelligence for Homeland Security and Personal Safety* (Piscataway, NJ: IEEE) pp 56–9

[23] Mazzeo P L, Ancona N, Stella E and Distante A 2003 Visual recognition of hexagonal headed bolts by comparing ICA to wavelets *2003 IEEE Int. Symp. on Intelligent Control* (Piscataway, NJ: IEEE) pp 636–41

[24] Blei D M, Ng A Y and Jordan M I 2003 Latent dirichlet allocation *J. Mach. Learn. Res.* **3** 993–1022

[25] Feng H, Jiang Z, Xie F, Yang P, Shi J and Chen L 2014 Automatic fastener classification and defect detection in vision-based railway inspection systems *IEEE Trans. Instrum. Meas.* **63** 877–88

[26] Wei X, Yang Z, Liu Y, Wei D, Jia L and Li Y 2019 Railway track fastener defect detection based on image processing and deep learning techniques: a comparative study *Eng. Appl. Artif. Intell.* **80** 66–81

[27] Liu J, Huang Y, Zou Q, Tian M, Wang S, Zhao X, Dai P and Ren S 2019 Learning visual similarity for inspecting defective railway fasteners *IEEE Sens. J.* **19** 6844–57

[28] Engelberg T and Mesch F 2000 Eddy current sensor system for non-contact speed and distance measurement of rail vehicles *WIT Trans. Built Environ.* **50**